TEG design for waste heat recovery at an aviation jet engine nozzle

Pawel Ziolkowski [1,*], Knud Zabrocki [1] and Eckhard Müller [1, 2]

[1] German Aerospace Center – Institute of Materials Research, Linder Höhe, Köln, Germany
[2] Institute of Inorganic and Analytical Chemistry, Justus Liebig University Gießen, Heinrich-Buff-Ring 17, 35392 Gießen, Germany
* Correspondence: pawel.ziolkowski@dlr.de; Tel.: +49-2203-601-3576

Abstract: The application of thermoelectric generators (TEG) on the nozzle of an aviation jet engine was studied by finite element TEG-simulations. Against the background of system-level requirements of the reference aircraft this work reports the resulting requirements on the TEG design with respect to applied thermoelectric (TE) element lengths and fill factors (F) within the TE modules in order to maintain a positive effect on the specific fuel consumption. Assuming a virtual optimized TE material and varying the convective heat transfer coefficients at the nozzle surfaces this work reports the achievable power output. System-level requirement on the gravimetric power density (> 100 Wkg^{-1}) can only be met for $F \leq 21\%$. Extrapolating TEG coverage to the full nozzle surface, the power output reaches 1.65 kW per engine. Assessment of further potential is demonstrated by a parametric study on the fill factor, convective heat transfer coefficients, and materials performance. This study confirms a feasible design range for TEG installation on the aircraft nozzle with a positive impact on the fuel consumption. This application translates into a reduction of operational costs, allowing for an economically efficient installation of TEG in consideration of the cost-specific power output of modern thermoelectric materials.

Keywords: thermoelectric generator, energy conversion, energy harvesting, aviation, jet engine, specific fuel consumption, module design, fill factor, FEM, simulation

1. Introduction

Thermoelectric generators (TEG) convert heat into electrical energy [1] without the loop of performing mechanical work in between, which makes them a favorable choice for energy harvesting applications in terms of robustness and reliability. The efficiency of thermoelectric (TE) conversion is determined on the material level by the figure of merit ZT, which is formed by the Seebeck coefficient S, and the electrical and thermal conductivity σ and κ, respectively ($ZT = S^2 \cdot \sigma \cdot \kappa^{-1}$). The TE conversion of waste heat has been considered in the past for high power generation in many fields such as for the supply of space probes [2,3], or automotive [4-6] and stationary applications [7,8]. In contrast to this, TE energy harvesting for aviation was dominantly taken into account in the past for low power applications to supply sensor nodes. Many works have been conducted in the context of structural health monitoring [9-11], whereby a proof of principle could already been given during flight tests according to a few reported studies [12,13].

Since the performance of aero-engines is already exploited to a high extent and further improvement by means of known concepts seems increasingly difficult, new technologies have to be considered in order to reduce the fuel consumption and environmental pollution of future aircrafts and to move closer to the specified goals by ACARE [14] and Flightpath 2050 [15]. For this reason more attention is payed recently to the recuperation of engine waste heat [16,17]. Conducted works on TE high power applications in the hot gas environment have been restricted over the years to basic assessments from estimated temperature differentials and approximated heat flux conditions [18-20]. These studies led to reserved conclusions on the resulting performance and postulates of a lacking technological and economic efficiency of TEG. Although admittedly lower in today's achievable efficiencies, TEG still avoid additional complex thermodynamic cycles, corresponding installations and their handling for the jet engine system. This principally corresponds to an easier implementation and lower maintenance effort compared to other emerging heat engine technologies (e.g. Organic Rankine Cycle). However, an increased areal coverage by TEG to maximize the efficiency and power output is still difficult especially on hot engines sections (high and low pressure turbine, combustion chamber) due to the typical configuration of jet engines, which offers only a limited installation space. Thus, the installation of the TEG between the hot core stream and the cool bypass flow was investigated in detail for an

application at the engine nozzle. While this implementation is certainly subjected to less design constrains it poses the drawback of lower temperature differentials applicable for the TEG.

In order to give the answer to the question, if a nozzle-mounted TEG could contribute to a reduction of the fuel consumption, combined numerical methods have been applied to forward simulation data to a parametrical model of the aircraft using the Pacelab Aircraft Preliminary Design (APD) software environment [21]. As the reference engine, a 2nd generation geared turbofan engine with an unmixed nozzle and design-freeze in 2030 was chosen together with an appropriate mission profile [22]. The most influential parameters of today's civil turbofan engines (bypass ratio, overall pressure ratio, turbine entry temperature, etc.) have been extrapolated the meet the prospective technology level in 2030 [23]. For definition of the geometry and the engine thrust requirements the engine was designed with GasTurb [24] for top of climb as design point (DP). By this, the resulting geometrical flow paths have been sized allowing for the study of operational behavior of the engine by variation of engine power settings. As described in a previous work [22], the heat transfer calculation at the nozzle was accomplished by solving the three-dimensional (3D) Reynolds-averaged Navier–Stokes (RANS) equations using the computational fluid dynamics (CFD) solver TRACE [25-27]. Equivalence of the fluidic and thermal boundary layer thickness was assumed for the calculation of the heat transfer coefficients of the boundary layers, corresponding to a Prandtl number = 1. The results of the CFD calculation were forwarded to a one-dimensional (1D) MODELICA model including the TEGs for computation of the heat flow from the core to the bypass. This process was repeated iteratively for precise calculation of the heat transfer at the nozzle. Based on the results on the heat flux a sensitivity analysis on the thermoelectric figure of merit *ZT* was accomplished for the evaluation of the fuel saving potential by means of a mission-based performance modelling of the aircraft using the Pacelab APD environment [28].

According to the aforementioned works the fuel saving potential of a TEG is given for two reasons. First, the generation of electrical energy by the TEG allows a slight mass reduction of the shaft-driven electric generator within the engine (1 kg/kW_{TEG}). The lowered mechanical power off-take of the generator from the driving shaft translates into an efficiency improvement and this in turn to a reduction of the specific fuel consumption (SFC). According to the APD model of the reference aircraft the maximum saving on SFC equals 1% for a totally reduced mechanical power off-take of the conventional generator (total replacement by TEG). In this case the TEG is supposed to deliver the entire average power output of the generator, which is set in correspondence to the APD model to 45 kVA per engine. Secondly, due to the heat transport from the hot core stream to the cool bypass flow the bypass boundary layer is accelerated, whereas the core boundary layer is decelerated. For top-of-climb and at cruise conditions the effect on the bypass flow shows an outweighing impact on the propulsive efficiency of the aircraft with a maximum improvement in SFC of approximately 0.1%.

The SFC improvement yields a saving of fuel mass, which can be traded with the additional mass introduced by the TEG. The break-even is reached on the aircraft level if the fuel efficiency improvement outweighs the weight impact of the TEG. According to the mission-based APD evaluation a fuel efficiency improvement is already given for a gravimetric electrical power density of the TEG > 173 Wkg^{-1} ("APD" limit) if one considers only the positive effects connected to the aircraft generator [28]. If the additional impact on the propulsive efficiency due to the heat transfer from the core to the bypass flow is taken into account, the requirement on the specific power density of the TEG reduces to 100 Wkg^{-1} ("APD+CFD" limit).

Although the implementation of a TEG with the specified power density will improve fuel efficiency, it will reduce the maximum range of the aircraft due to the limitation on the maximum take-off weight (MTOW) of the aircraft. In order to reach a range invariant implementation of TEG an increased electrical power density > 520 Wkg^{-1} ("APD range-invariant" limit) is required according to the aircraft model.

Thermal boundary conditions from the CFD model have been transferred to a finite element model (FEM) of a thermoelectric double leg in this work. Operational characteristics of this double leg have been extrapolated to a full coverage of the nozzle surface with the specified geometry from GasTurb. Parametric studies on the TEG design have been conducted in order to verify the viability to satisfy the gravimetric power density requirements on aircraft level and to specify requirements on the TEG design and its resulting performance.

2. Materials and Methods

The modelling is accomplished on a thermoelectric double leg by a 3D steady state temperature dependent FEM simulation using ANSYS Workbench™. Though simulation was conducted for all flight phases of the chosen mission profile, the geometry optimization and detailed performance calculations have been performed

for the cruise phase, which has the highest temporal share (87%) of the total mission time (395 min.) for the set flight distance of 2850 NM. Starting from material properties, measured on n- and p-type Skutterudite samples, high performance virtual materials (HPVM) are created by modification of the temperature characteristics of the TE transport properties. More details on the individual TE transport properties can be found in the supporting information within the appendix of this publication (Fig. A1).

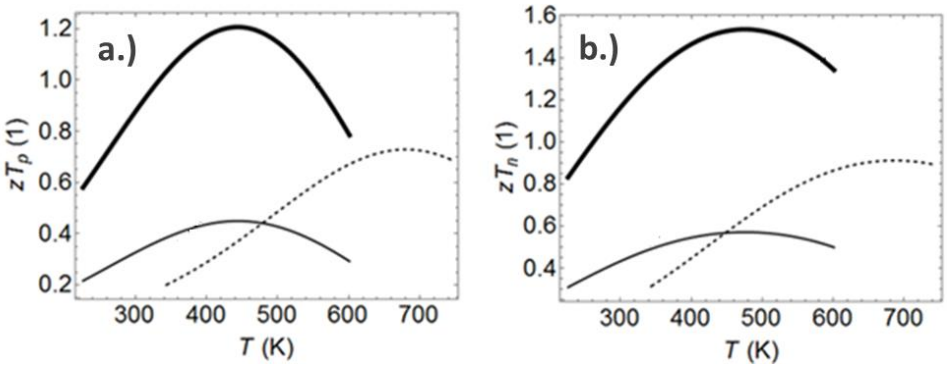

Figure 1. Figure of merit *ZT* of a virtual p-type (a.) and n-type (b.) thermoelectric material for simulation. The dashed lines represent fits of measured properties on Skutterudite samples. Curves shown by light solid lines show the temperature course of *ZT* after the shift of transport properties into the temperature range of the nozzle application is applied. Bold solid lines show the *ZT* characteristic of the virtual material, which is considered for the simulation.

First the characteristic of the thermal conductivity, the Seebeck coefficient and the electrical conductivity of the Skutterudite materials is each shifted into the temperature range of the nozzle application in order to represent the use of an optimized material. As an effect of the lower mean temperature the resulting *ZT* values decrease. To consider a reasonable technology level of a future TE material during simulation, the power factor ($PF = S^2 \cdot \sigma$) of the p- and n-type material is increased by an improvement of the Seebeck coefficient and the electrical conductivity by 40% for each property. In order to receive a realistic performance assessment an additional decrease of thermal conductivity is not chosen in first attempt, since the originally measured data already corresponds to filled Skutterudites with low thermal conductivity. Finally, the HPVM with peak *ZT*-values of 1.2 (p-type) and 1.5 (n-type) are used as the baseline for the simulation. In consideration of the temperature range for the nozzle application, these characteristics correspond to a reasonable $ZT_{mean} = 1.14$ for the connected double leg configuration.

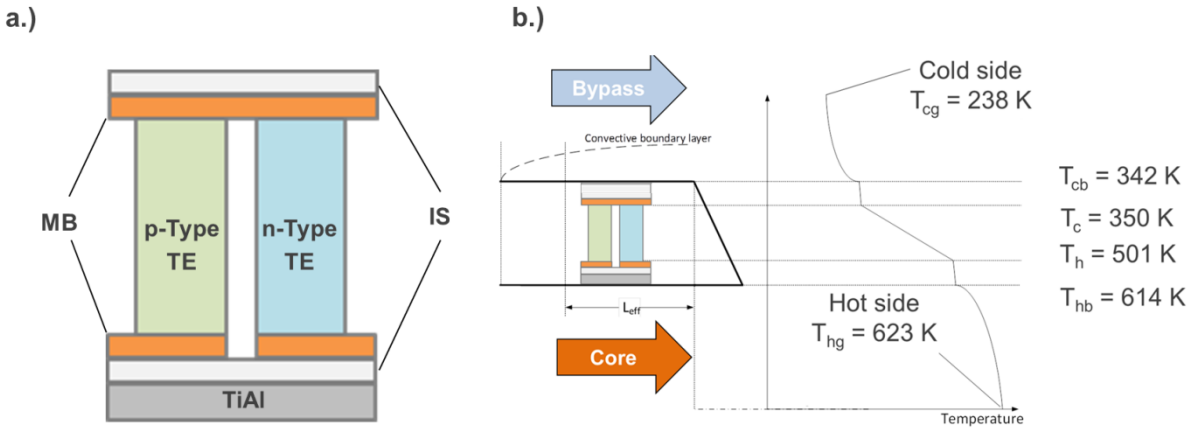

Figure 2. Scheme of the thermoelectric double leg configuration composed of isolation layers (IS), metallic bridges (MB), the p- and n-type TE material legs, and the TiAl nozzle (a.). Schematic of the installation at the aircraft nozzle and exemplary temperature distribution along the heat transmission path for $F = 25\%$ (b.).

The operational characteristics of the TEG are simulated for a double leg configuration (Fig. 2) under consideration of all relevant effects like Joule heating, and the thermoelectric Peltier, Seebeck and Thomson effect. The nozzle of the aircraft is modelled by a layer on the outside of the 3D configuration. Due to weight minimization the nozzle is supposed to be made from TiAl with a temperature dependent thermal conductivity

between 20–30 $Wm^{-1}K^{-1}$ [29]. With 2 mm the thickness of the TiAl is chosen in accordance with the original design of the nozzle body. Flat surfaces are considered for external heat exchange with the air flows. Due to the major sensitivity of the propulsive efficiency on the flow condition at the cold bypass boundary layer [23] only modification of the hot nozzle surface seems viable for any optimization of convective heat transport. In order to minimize temperature losses at the cold bypass side too, a direct incident flow on the isolation layer of the thermocouple is assumed here. Thus, the nozzle layer was modelled only for the hot core stream. For reduction of parasitic temperature drops a layer of AlN with a high thermal conductivity of 170 $Wm^{-1}K^{-1}$ [30] is introduced to form an electrical insulation between the TE double leg and the metallic nozzle. Considering the dielectric strength of AlN of 20 $kVmm^{-1}$ [31], a minimum thickness of 325 µm is set for this layer on both sides with regard to weight optimization and concurrent electric insulation effect in presence of high DC voltages generated by the entire TEG at the nozzle. Metallic Cu bridges with a thickness of 200 µm form the electrically connecting bridges between the TE elements. TE elements are simulated for square-shaped cross sections with a foot print of 1x1 mm^2 for each leg. The spacing between the legs is set to 1 mm. The variation of the fill factor is accomplished by modification of the nozzle and isolation surfaces, respectively, which are supposed to provide the heat exchange with the external air flows. The length of the legs is varied in order to obtain a match of the thermal resistance of the TE thermocouple in relation to the outside resistances within the heat transmission path. An aerogel filling for the voids of the configuration is assumed as thermal insulating material with a reasonable assumption for its thermal conductivity of $30 \cdot 10^{-3}$ $Wm^{-1}K^{-1}$ [32,33] in order to minimize parasitic heat bypasses within the TE module. Neither radiative nor convective heat transport was assumed within the aerogel-filled voids of the double leg configuration.

According to the CFD simulation the gas temperatures of the core and the bypass flow are T_{hg} = 623 K and T_{cg} = 238 K, respectively, during cruise conditions. The simulations revealed considerably high thermal resistances within the heat transmission path due to relatively low heat transfer coefficients (HTC) of the convective heat exchange between the air flows and the nozzle and isolation surface (Fig. 3), respectively. The convective heat transfer is considered at the particular surfaces by appropriate settings of the calculated HTC and the respective gas temperatures from CFD simulations within the thermocouple model.

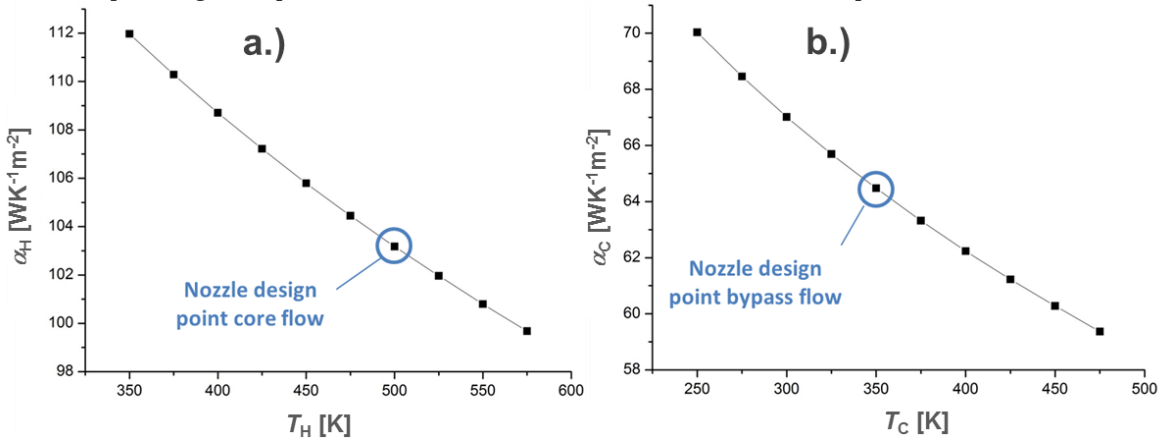

Figure 3. Temperature dependent convective heat transfer coefficients at the hot core stream (a.) and the cool bypass flow (b.). The depicted design points indicate values, which have been determined for a thermoelectric module with a fill factor F = 25% and an adjusted length of the thermoelectric legs of 21.2 mm for matching of thermal resistance.

An electrical DC current is applied on the terminals of the double leg for determination of the electrical power output. While varying the electrical current from zero to the short circuit current for the actual design, the simulation of the terminal voltage allows for the determination of the maximum output power for the particular application condition. Efficiency of the double leg is calculated from the ratio of power output to the incident heat flow of the double leg.

The heat flow on the hot and cold side of the double leg configuration reveals a spatial distribution due to different thermal conductivities of the virtual p- and n-type material (Fig. 4). Discrete data on the amount of the heat flux vector (normal component) is taken at every node of the surface for areal interpolation and subsequent approximation by a continuous area function. The incident heat flow is finally determined by integration of this function over the entire top surface of the hot side.

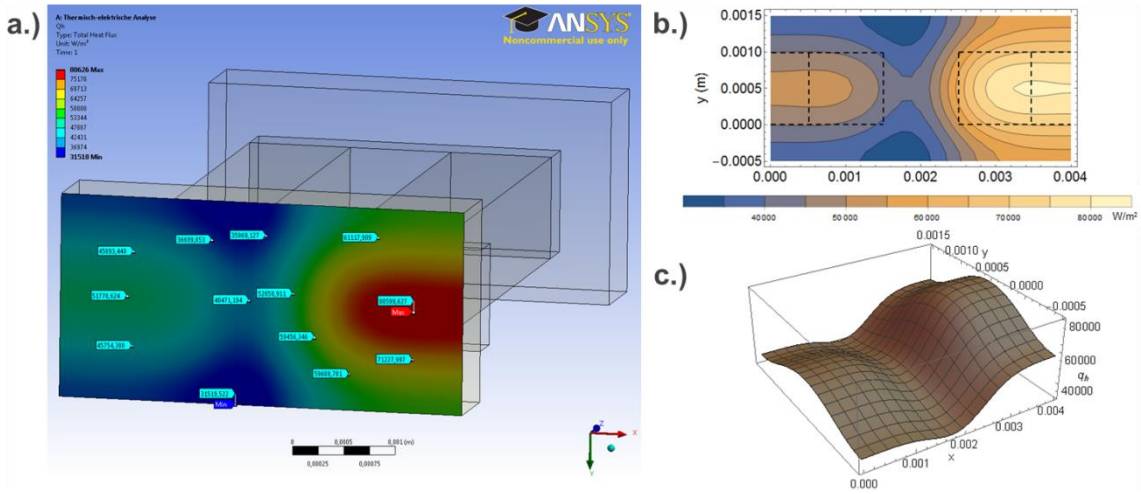

Figure 4. Qualitative heat flow distribution on the hot side of the thermocouple for an exemplary set of boundary conditions and geometrical thermocouple design (a.), areal interpolation of discrete node data on the normal component of the heat flux vector (b.), and continuous area function of the heat flux on the hot side (c.).

With regard to the system-level requirements on the gravimetric power density further assumptions on the density of the different components are made (Table 1). Considering light-weight silicide TE materials and contributions from the other components of the simulated configuration, the mass of the thermocouple is calculated, which equals for instance 187 mg for the design case with F = 25% at its optimal TE leg length of 21.2 mm (Table 1).

Table 1. Material, geometry G, volume V, density ρ, and mass m as properties of different components of the thermoelectric double leg configuration. The values are representative for a thermocouple design with a fill factor of F = 25% and an adjusted length of thermoelectric legs of 21.2 mm for matching of thermal resistance.

Part	Material	G [mm]	V [mm³]	ρ [gcm^{-3}]	m [mg]
Isolation	AlN	2 x 4 x 0.325	2 x 2.6 = 5.2	3.2	16.6
TE	Mg_2Si	1 x 1 x 21.2	2 x 21.2 = 42.4	2.3	97.52
Bridge	Cu	1 x 3 x 0.2	2 x 0.6 = 1.2	8.92	10.7
Nozzle	TiAl	2 x 4 x 2	16	3.9	62.4

For every studied parametric case the thermal resistance of the thermocouple is matched with the sum of the effective heat resistances by convection plus the minor contributions of the TiAl and AlN layers by variation of the TE leg length in the range between 1 mm and 25 mm. First calculations are conducted for a typical thermocouple design for a today's bulk-based TE module with a fill factor F = 25% using the HPVM (case 1 in Table 2). An assessment on the achievable power output for higher TE material performance compared to the HPVM is accomplished by increasing the power factor of the HPVM in three steps by 10%, yielding a ZT_{max} of 1.56 and 1.95 for the supposed p- and n-type material, respectively, at the last step (case 2).

In order to optimize the gravimetric power density without increase of the materials performance further simulations are carried out on the base of the HPVM but with smaller fill factors F (case 3), which yields a reduction of the thermal convection resistances on both sides of the thermocouple. Reduction of F is accomplished within the model by increasing the TiAl and AlN surfaces on both sides of the air flows. Additionally the effect of a presumed improvement of the convective heat transfer on the hot side is studied by choosing a higher HTC α_H compared to the outcome of the CFD simulations within every simulated parameter configuration of the model. The increase of α_H reflects a hypothetic modification of the nozzle surface for an improved aerodynamic design, which is not optimized concerning its heat transfer in this study at all. However, room of further improvement on the heat exchange at the hot side is indicated by a certain insensitivity of the propulsive efficiency of the engine to the fluidic conditions at the core stream boundary layer [23]. The situation differs significantly at the cold bypass flow, and seems to give apparently much less space for heat exchange optimization. In order to maintain the detected positive effect on the propulsive efficiency from the acceleration of the bypass boundary layer, the HTC on the cold side is set to α_C = 64 WK^{-1}m^{-2} for all discussed cases in this work. This value represents a flat surface design at the cold bypass flow, as it was assumed in the CFD

calculations, which shall not impose a restriction for further optimization of heat exchange by e.g. vortex-generating or lamellar surface structures, however. Additional studies are needed in the future to identify the possibilities for an improved convective heat exchange at the bypass flow of the nozzle with concurrent minimal repercussions on the engine operation and maintenance of positive effects on the propulsive efficiency after implementation of the TEG. For the sake of completeness further simulation results for a model with higher cold side HTC can be found in the supporting information within the appendix of this publication (Fig. A2). Summarizing, Table 2 gives a survey on the cases and their respective parameter ranges, which will be discussed later on in this publication.

Table 2. Simulation cases with their considered parameter ranges for different model properties: Hot and cold side heat transfer coefficient α_H and α_C, fill factor F, leg length l_{TE} and ΔPF as the change of the power factor compared to the baseline material properties of the high performance virtual material (HPVM). $\Delta PF = 0$ indicates the use of the HPVM as defined in Fig. 1 and Fig A1 in the supporting information within the appendix, respectively.

Case	α_H [$WK^{-1}m^{-2}$]	α_C [$WK^{-1}m^{-2}$]	F [%]	l_{TE} [gcm^{-3}]
1	100 - 500	64	25	1 - 25
2	100 - 500	64	25	1 - 25
3	100 - 500	64	3 - 25	1 - 25

For determination of the TEG performance the thermocouples are supposed to be connected to TE modules (TEM) with a footprint of 50x50 mm². With the given cross section of 1 mm² of each TE leg the footprint of one thermocouple equals A_{TC} = 8 mm² (1 mm spacing between each leg) for F = 25%. With this fill factor 312 thermocouples can be connected within one TEM, yielding a total area covered by the TE legs of A_{TE} = 624 mm² per TEM.

Table 3. Number of thermocouples, area per thermocouple A_{TC}, and active area covered by thermoelectric legs within a 50 x 50 mm² thermoelectric module A_{TE}, each classified according the fill factor F

Property	F = 25%	F = 12.5%	F = 6.25%	F = 3.125%
TC Number [-]	312	156	78	39
A_{TC} [mm²]	8	16	32	64
A_{TE} [mm²]	624	312	156	78

The coverage by TEM was extrapolated to the full nozzle surface (Fig. 5). According to the GasTurb engine design a total surface $A_{noz} \cong 1.1$ m² is available for the TEG installation at the nozzle, which gives space for 442 TEM per engine. A possible implementation encompasses a TEM alignment within 13 rings á 34 modules around the nozzle body. Simulations of the thermal conditions at the nozzle revealed a radial symmetric temperature distribution. However, a minor axial temperature variation along the nozzle, which is confirmed to be < 11 K for cruise conditions, was not considered for the simulations on the TEG design and resulting power of the overall system at the nozzle.

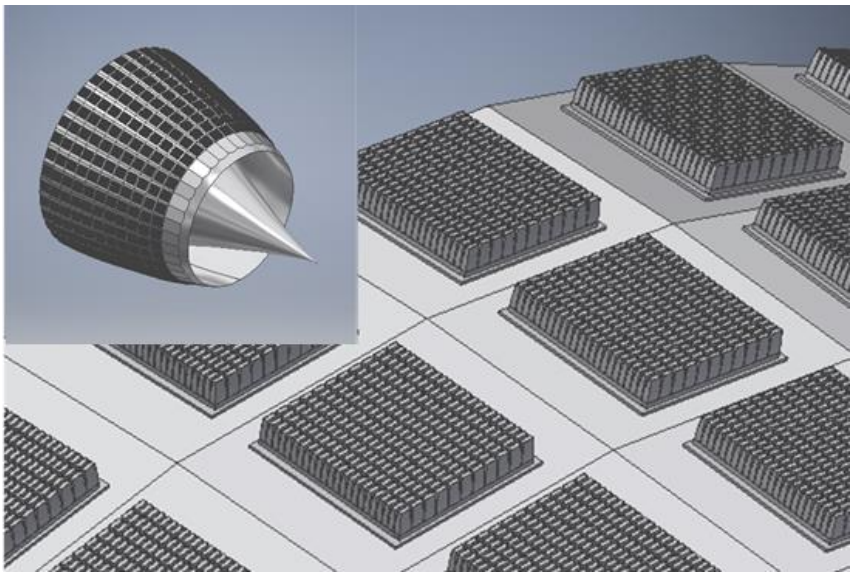

Figure 5. Example for an occupation of the nozzle surface by TEM[1]. The shown design implies the application of vertical bars for improved heat exchange at the bypass flow, which is not considered in the simulation. Inset: Overall vision of TEM alignment on an aviation nozzle.

3. Results

Due to the thermal resistance of the convective boundary layers at the core and bypass flow only a fraction of the gas temperature difference can be used at the TE material, which limits the maximum power output and efficiency of the thermocouple. In presence of external thermal resistances the temperature difference at the TE material is a function of the leg length. For small leg lengths the reduced thermal resistance of the TE leg yields a high incident heat flow but low temperature difference across the legs. Consequently the power output and the efficiency become low too. Though high leg lengths provide an increase of the temperature difference, the increasing thermal resistance of the thermocouple lowers the incident heat flow, which yields a reduction of the power output above a certain leg length due to the given efficiency of the TE materials.

[1] Courtesy of Fabian Ahrendts, TU Braunschweig.

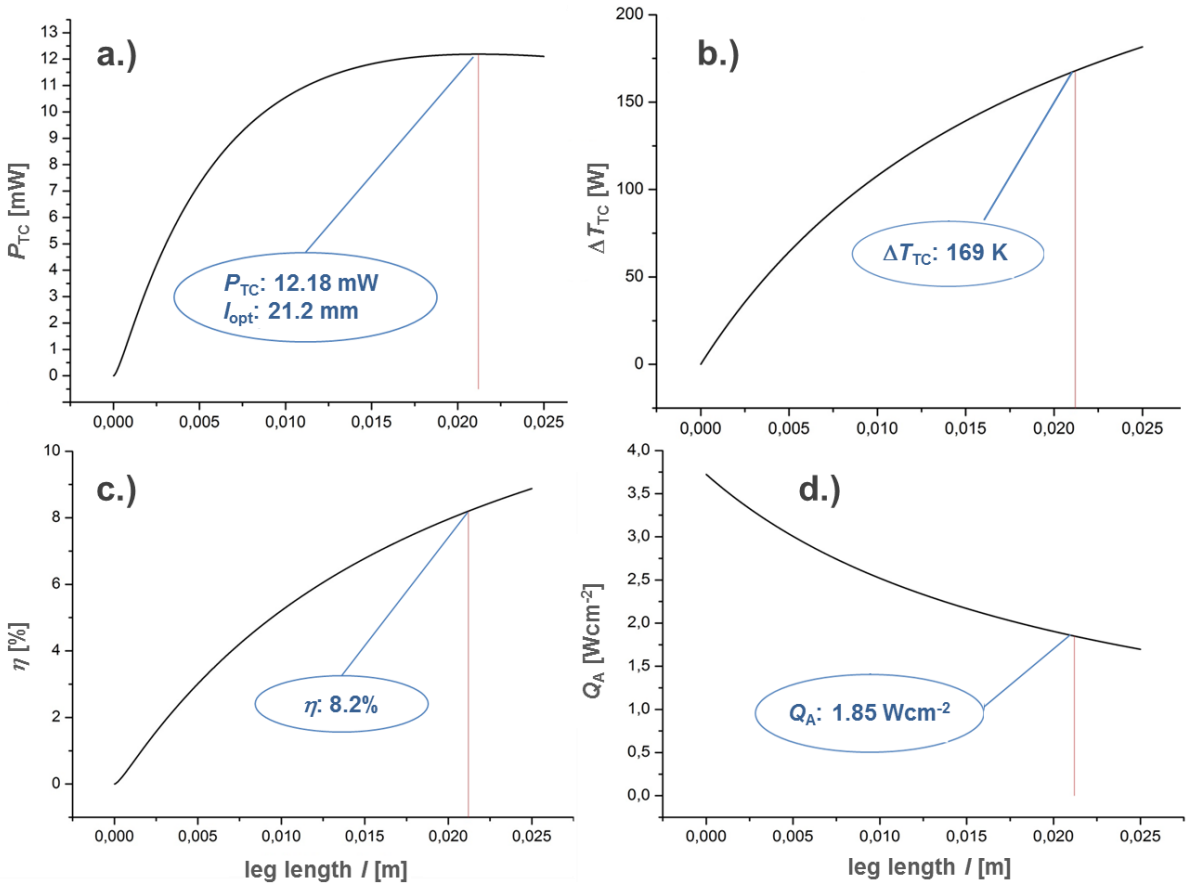

Figure 6. Simulation results of a thermocouple with F = 25% and for convective heat transfer coefficients of α_H = 100 WK^{-1}m^{-2} / α_C = 64 WK^{-1}m^{-2}. Fitted power output (a.), temperature difference (b.), efficiency (c.), and hot side heat flux density (d.) as functions of the leg length.

Maximization of the TEG performance is accomplished by choosing an optimal leg length in order to match the thermal resistance of the thermocouple with the sum of external thermal resistances within the heat transmission path [34], which is represented here by the convective heat transfer, the nozzle and isolation layers. This yields the best compromise between the temperature difference at the TE material and the incident heat flow to the thermocouple. For the set HTC at both boundary layers (α_H = 100 WK^{-1}m^{-2} / α_C = 64 WK^{-1}m^{-2}) the optimal leg length for maximised power output equals l_{opt} = 21.2 mm at F = 25% (Fig. 6). Each thermocouple contributes 12.18 mW to the total power output of the TEM working at a temperature difference of 169 K across the TE legs. Considering the resulting heat flux, the efficiency equals η = 8.2%, which is a result of the optimized HPVM with its fitted temperature characteristic of transport properties with regard to the application temperature range. With the assumptions made on geometries and chosen material properties the entire TEG exhibits the following operational characteristics at the nozzle.

Table 4. Mass m, maximum power output P_{max}, gravimetric power density P_G, and areal power densities for a HPVM-based TEM with F = 25% at α_H = 100 WK^{-1}m^{-2}, and α_C = 64 WK^{-1}m^{-2}. P_{A_TEM} relates the areal power output to the total footprint of the TEM, while P_{A_TE} is the ratio between power output and the active surface of the TEM occupied by TE legs only. Values for mass and power output are scaled up for the entire TEG at the nozzle, which consists of 442 TEM.

F = 25%	m [g]	P_{max} [W]	P_G [Wkg^{-1}]	P_{A_TEM} [Wcm^{-2}]	P_{A_TE} [Wcm^{-2}]
TEM	58.4	3.8	65.06	0.152	0.61
TEG	25812.8	1679.67			

Increasing α_H from 100 WK^{-1}m^{-2} to 500 WK^{-1}m^{-2} on the hot side of the model yields a reduction of the optimal leg length for satisfaction of the thermal match condition and in turn to an increase of the incident heat

flux (Fig. 7a). The lower mass translates into a higher gravimetric power density, which is likewise achievable by an assumed growth of the *PF* (Fig. 7b).

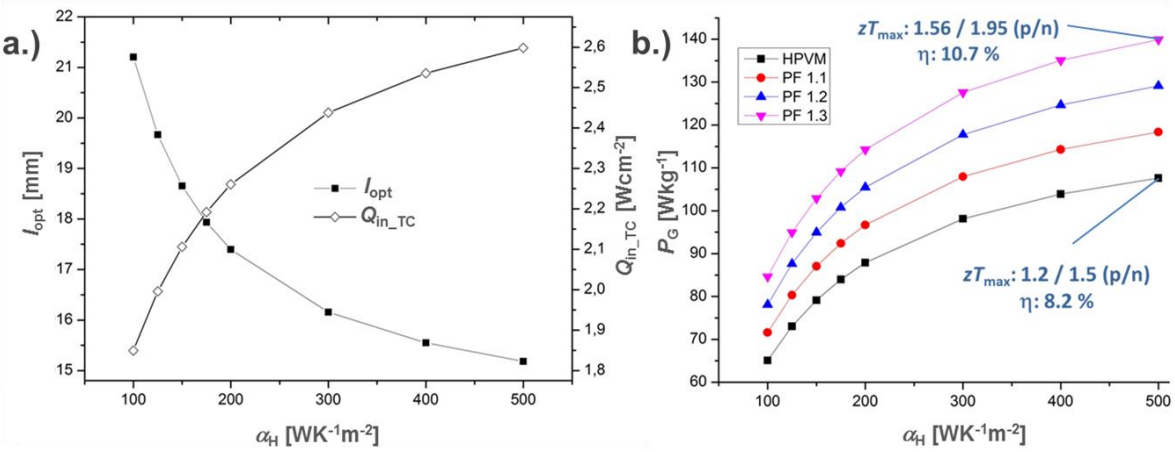

Figure 7. Optimal leg length and heat flux (a.) and gravimetric power density (b.) as a function of the hot side HTC α_H. The gravimetric power density is shown for the HPVM and for an increased power factor *PF* of the HPVM by three steps of 10% each.

Increasing the surface for the convective heat exchange per thermocouple on both sides effectively decreases the thermal resistance of the convective boundary layers. The lower *F* yields the reduction of the optimal leg length for matching of thermal resistances, which allows for a significant mass reduction (Fig. A3).

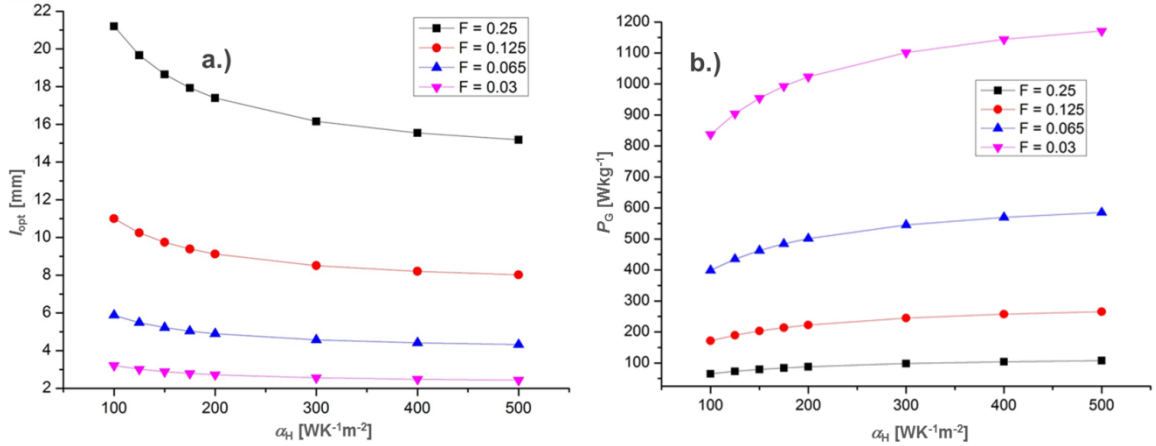

Figure 8. Optimal leg length l_{opt} (a.) and gravimetric power density *PG* (b.) as a function of the hot side heat transfer coefficient α_H for different fill factors *F* of the thermocouple.

The incident heat per thermocouple grows as a consequence of the reduced thermal resistance of the convective boundary lavers and TE legs (Fig. A4). The reduction of *F* increases the gravimetric power density significantly (Fig. 8b). While the minimum requirement for a positive effect on the SFC is determined by the resulting gravimetric power density P_G of the TEG, the amount of SFC saving scales with the total electrical power output delivered from thermoelectric recuperation. Due to the limited installation space, the power output is linked to the areal power density P_A of the TEG (Fig. 9).

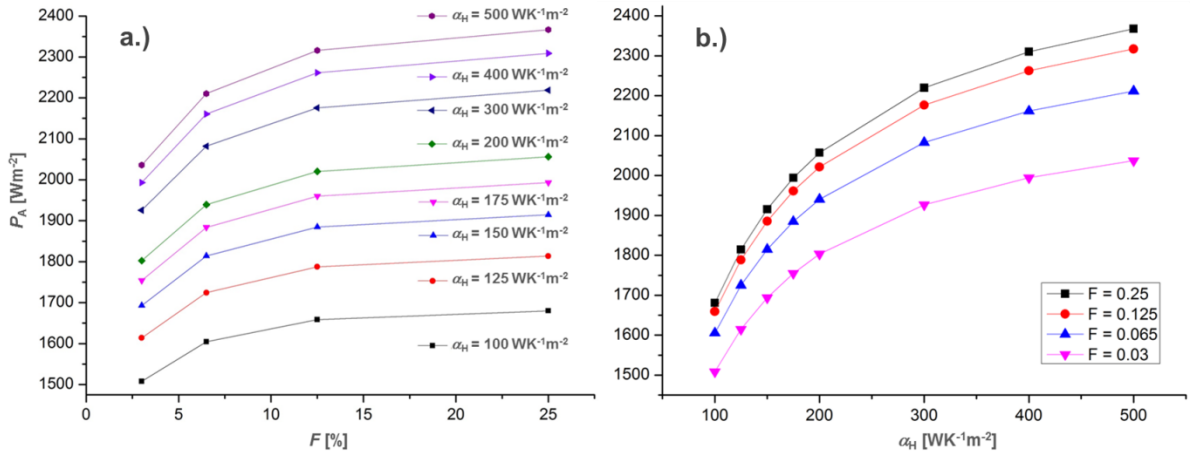

Figure 9. Areal power density P_A as a function of the fill factor F for different HTC α_H (a.). Converted data of P_A in dependence of α_H for different F (b.).

4. Discussion

The presence of MW heat losses of turbofan engines [35] in contrast to relatively low average electrical power requirements of today's mid-size aircrafts (180 PAX ~ 45 kVA/engine) offers an attractive fuel saving potential from a direct conversion of engine heat into electrical energy by TEG at first glance. As shown in a previous work [22], the assumption of an efficient heat transfer by heat pipes (κ_{eff} = 400 Wm^{-1}K^{-1}) and conservative TEG material efficiency (ZT_{mean} = 0.8) yields a specific TEG power output between 1 kWm^{-2} to 9 kWm^{-2}, which becomes attainable from of a first approximation of temperatures and heat fluxes on the five studied sections of the reference engine: high- and low pressure turbine (HPT, LPT), interducts, and nozzle. Consideration of the theoretically maximum available surface of the turbofan geometry would allow for an installation of approximately 15 kVA TEG power output per engine in total. However, the installation of TEGs on high temperature sections of the engine (HPT, LPT) seems technically difficult, which favors an implementation at the nozzle. A detailed analysis of the fluidic and thermal conditions revealed high convective thermal resistances as the main bottleneck for performant TEG operation at the nozzle.

Using the HPVM with F = 25% and optimized leg length, a minimum α_H > 350 WK^{-1}m^{-2} is required to fulfil the "APD+CFD"-limit of 100 Wkg-1, while the requirement of the "APD"-limit (173 Wkg-1) and the limit for a range invariant TEG installation (520 Wkg-1) are not achievable at all (Fig. 7b). Increasing the PF of the HPVM by 30% at α_H = 100 WK^{-1}m^{-2} does not fulfil the criteria for a beneficial TEG installation, too. Generally the Increase of α_H reduces the thermal resistance within the heat transmission path, allowing for a reduced leg length and mass saving for the configuration. Varying α_H from 100 WK^{-1}m^{-2} to 500 WK^{-1}m^{-2} yields a reduction of the optimal leg length by 30%, which translates into reduction of thermocouple mass of 6.6%. Due to the matching of thermal resistances the effective temperature difference at the TE legs remains almost constant, while the heat flux increases significantly for smaller leg lengths, yielding an increase of gravimetric power density. Due to an unchanged α_C the mean temperature rises along the thermocouple with increasing α_H. Since the material properties are fixed with regard to their initially set temperature range, a higher mean temperature yields a continuously increasing bipolar contribution due to the approach to the intrinsic temperature domain of the supposed TE properties. In connection with non-vanishing temperature losses at the boundary, nozzle and isolation layers this yields a flattening of power density curves at higher α_H, irrespective of the lower optimal leg lengths. Since the minimal gravimetric power requirement of the aircraft system of 100 Wkg^{-1} is only satisfied at F = 25% by an improved convective heat exchange with a concurrent significant increase of materials performance, it is apparently not expedient to apply TE modules with higher fill factors for the application at the aircraft nozzle.

Future TE materials are likely expected to have maximal ZT-values ~ 2 for technologically relevant and stable material classes from today's point of view. Against this background and in conjunction with reasonable assumptions on the performance for the convective heat exchange at the nozzle a beneficial TEG application is attainable only for smaller fill factors. However, the minimum applicable fill factor F_{min} is limited for several reasons. First, the spreading resistance of components for heat conduction within the heat transmission path can

lower the effective temperature difference at the TE materials, since heat has increasingly to be provided laterally through substrates or isolation layers to the thermocouple legs at low F. For instance the United States National Aeronautics and Space Administration (NASA) demonstrated the feasibility of F = 3.4% within their GPHS-RTG [36] and even lower values for F_{min} = 1% have been suggested as a practical limit, once materials with high thermal conductivity are used to connect the thermocouples to external heat exchangers [37].

Secondly, F_{min} is limited due to the reduction of necessitated leg lengths for matching of thermal resistances. A decreasing leg length puts higher requirements on the electrical contact resistance between bridges and the TE legs in order to maintain a high power output of the TEM at low F. At typical values for the electrical conductivity of TE materials (~10^3 Scm^{-1}) contact resistances between 10^{-6} – 10^{-5} Ωcm^2 allow for a reduction of the leg length down to 0.1 mm, which was already successfully demonstrated in commercial TE devices for cooling [38] and generator applications [39]. Additional simulations on the impact of electrical contact resistances during this work confirmed a necessitated contact resistance < 10 $\mu\Omega cm^{-2}$ in order to mitigate losses on the power output < 10% at the aircraft nozzle.

Finally the concurrent reduction of F and lower leg lengths promote a parallel heat flow through the voids of the thermocouple configuration, which can lead potentially to a significant reduction of the efficiency in case of convection or heat transport by radiation. For open or evacuated TEG the application of low-emissivity metallization layers has turned out to be an appropriate mean to reduce radiative heat exchange within TEMs. Using solid filling of voids by aerogel material, as considered by the simulation model of this work, effectively prevents parasitic thermal crosstalk between the hot and cold side of the thermocouple by convection. Selective simulations on the impact of the parasitic heat conduction through the aerogel revealed a maximum decrease of power output of 0.67%, which is supposed to be a tolerable value.

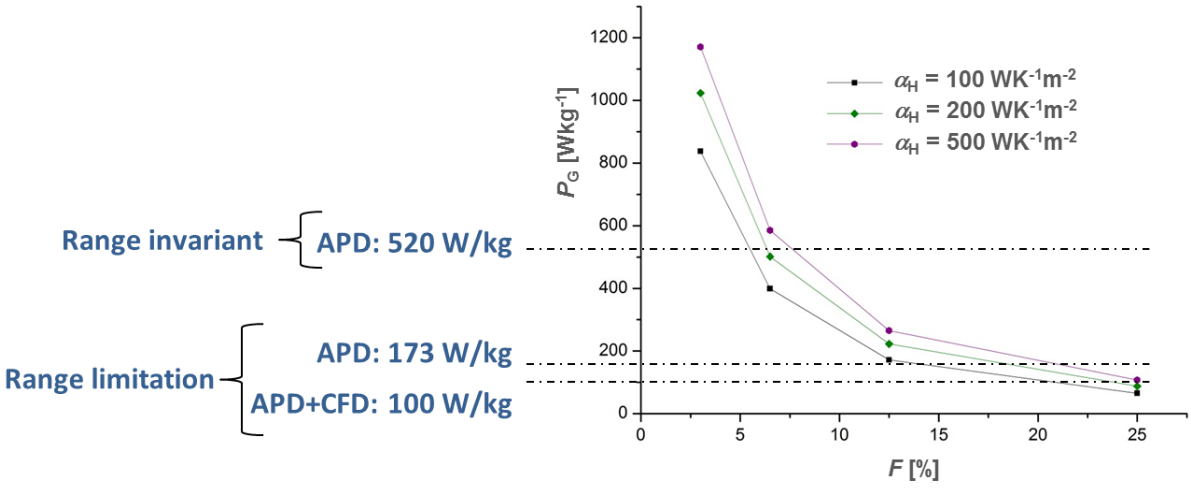

Figure 10. Gravimetric power density P_G of a HPVM-based TEM as a function of the fill factor F for different HTC α_H. PG is displayed together with the required level from the aircraft model.

Lowering the fill factor F yields a high mass saving due to significantly lowered thermal resistance of the convective boundary layers and reduced optimal leg lengths of the thermocouple. Reducing F from 25% to 3% reduces the thermocouple mass by 43% (Fig. A3). At the design point of the convection HTC parameters at the nozzle (α_H = 100 $WK^{-1}m^{-2}$, α_C = 64 $WK^{-1}m^{-2}$) the minimal gravimetric power density requirement ("APD+CFD"-limit) is fulfilled for the HPVM for F < 21% (Fig. 10). Considering only the positive impact on the reduced mass and power off-take of the engine generator ("APD"-limits) a beneficial installation of TEG becomes attainable for F < 12.4%, while access to a range-invariant TEG implementation is given for F < 5.5%, respectively. Improving the hot side convective HTC to α_H = 200 $WK^{-1}m^{-2}$ the power density requirements are fulfilled for slightly higher F. PG = 100 Wkg^{-1} is attainable for F < 23.8%, while the range-invariant installation requires F < 6.3%. According to the simulation results the range for maximum gravimetric power density at F = 3% is given between 800 Wkg^{-1} and 1200 Wkg^{-1} in dependence of α_H.

The decrease of mechanical power off-take by the generator scales with electrical power output of the TEG, while the positive impact on the propulsive efficiency by acceleration of the bypass flow is linked to the

heat flow dissipated by the TEG, which is likewise connected over the thermocouple efficiency to the power output of the TEG. Thus, the quantitative determination of the SFC saving requires the determination of the amount of electrical power provided by thermoelectric recuperation. Considering the limitation on the installation space the power output is determined by the achievable areal power density *PA* of the thermocouple. At $\alpha_H = 100\ WK^{-1}m^{-2}$ and $\alpha_C = 64\ WK^{-1}m^{-2}$ *PA* stays below 1680 Wm^{-2} independently from the fill factor applied. Reducing the fill factor from 25% to 3% yields a reduction of the areal power density in the range of 10% for a particular α_H (Fig. 9b). This is connected to the finite thermal conductivity of the components within the heat transmission path and the corresponding spreading resistances on both sides of the thermocouple configuration. Due to the low thicknesses of the nozzle and insulation layers, which are minimized in order to receive a maximized gravimetric power density, the components set a considerably thermal resistance for the lateral heat transport, which lowers the effective temperature difference at the TE materials. As a consequence the heat flux density decreases for a particular set of HTC by approximately 10% when *F* is reduced from 25% to 3% (Fig. A4).

For the design points of the HTC ($\alpha_H = 100\ WK^{-1}m^{-2}$, $\alpha_H = 64\ WK^{-1}m^{-2}$) and the set total surface (A_{noz} = 1.1 m²), which is offered for TEG occupation, a total power output between 1.65 kW and 1.85 kW can be expected from the thermoelectric recuperation at the nozzle for *F* = 21% and *F* = 3%, respectively. This corresponds to 3.6% to 4.1% of the average electrical power output of the shaft-driven electric generator within each engine of the reference aircraft.

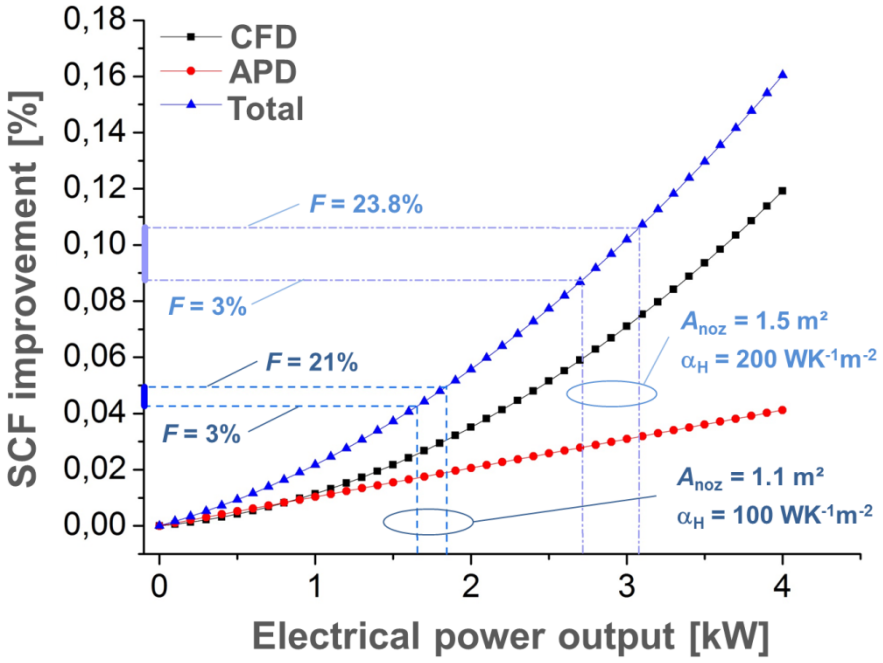

Figure 11. SFC improvement as a function of electrical power output of the TEG at the aircraft nozzle. The SFC is calculated on the base of data from [28]. Contributions from the bypass acceleration (CFD) and the reduced power off-take of the generator (APD) add to the total SFC reduction. Ranges of SFC improvement are highlighted for two different occupation surfaces at the nozzle with varied HTC α_H. The corresponding values of the electrical power output are calculated according to the respective areal power densities for the permitted ranges of *F*, which fulfil the minimum gravimetric power density requirement.

The power output for *F* = 21% of 1.85 kW offers a total SFC improvement of 0.05% (Fig. 11). Slightly lower SFC reduction of 0.045% is achieved at *F* = 5.5% but with the advantage of a range invariant installation of the TEG, as the gravimetric power density exceeds 520 Wkg^{-1}. A possibility to improve the SFC saving is given by an increase of the installation space, which is calculated for a higher value of A_{noz} = 1.5 m² additionally. Increasing simultaneously the performance of the convective heat transfer to $\alpha_H = 200\ WK^{-1}m^{-2}$ the corresponding areal power density offered by the TEG could allow for a SFC improvement of 0.11% at *F* = 23.8%. Again, slightly lower SFC reduction of 0.096% is achieved at *F* = 6.3% for a range invariant installation of the TEG at the geometrically extended nozzle. A further but not yet investigated mean to increase the power density is given by exchanging the TiAl by electrically isolating SiC. Due to higher thermal conductivity and

simultaneously lower density SiC could decrease the mass and the spreading resistance of the nozzle, while making the use of the AlN layer unnecessary, which would allow for an additional reduction of mass.

However, according to the simulation results a SFC saving between 0.05% and 0.1% seems plausible for the TE recuperation of waste heat at the engine nozzle. Though the nominal values might seem small, a considerable economic impact can be estimated from the beneficial impact on operational costs. According to estimations from Boeing [18] a SFC improvement of 0.1% translates into a cost saving of 2.4 Mio$/month for the entire US civil aviation sector. Own estimations [40] on the base of a 0.1% SFC improvement yield a potential saving of 144 k$ per airplane over a typical operation time of 28 years. Consequently a return of invest during five years could be attainable for a 2 kW TEG system within the cost limit of < 16 $/W. According to recent studies the sum of material and heat exchanger costs for modern TE materials can be estimated below 10 $/W for F < 10% and at operating temperatures between T_H = 700 K and Tc = 300 K [41], which might be relevant for a progressive approach of a high performant heat transport system at the nozzle with the use of heat pipes. Considering the total TE system costs (including manufacturing, heat exchanger and material costs for thermoelectrics and ceramics) values < 20 $/W are offered by a certain number of today's TE materials at the temperature range between T_H = 523 K and T_C = 293 K [42]. This opens a realistic window for an economically efficient installation of TEG in future, especially under consideration of further optimization potential concerning particular assumptions made within this simulation study.

5. Conclusions

FEM-based simulations are conducted for the application of a thermoelectric generator (TEG) between the hot core stream and the cool bypass flow at the nozzle of an aviation turbofan engine. Temperatures of the core stream and the bypass flow are derived from CFD results [23] and applied as boundary conditions to the FEM simulation of various thermocouple configurations. In conjunction with effective heat transfer coefficients (HTC) between the flat surfaces of the nozzle and the core (α_H = 100 $WK^{-1}m^{-2}$) and the bypass (α_C = 64 $WK^{-1}m^{-2}$) air flow, respectively, the performance of different thermocouple designs is simulated on the base of a virtual material with a ZT_{mean} = 1.1. Focus is placed on the identification of the appropriate fill factor F and TE element length in order to maintain a positive impact on the specific fuel consumption (SFC) of a reference aircraft [22]. The maximal gravimetric and areal power density of the TEG is simulated for 3% < F < 25% with a concurrent determination of the optimal leg lengths for matching of thermal resistances.

The requirement on the gravimetric power density, which was determined from of a parametric aircraft model [28], cannot be fulfilled for a thermocouple design with F = 25%, neither by an increase of the HTC nor by a reasonable improvement of materials performance. The minimum break-even point of gravimetric power density (100 Wkg^{-1}) for a TEG implementation with a positive impact on the SFC but with the drawback of a reduced flight range of the aircraft is attainable for F < 21%. The low HTC (α_H = 100 $WK^{-1}m^{-2}$, α_C = 64 $WK^{-1}m^{-2}$) of the convection heat exchange at the flat nozzle surface turned out to be the bottleneck for the maximization of the TEG performance. Consequently the requirement for a range-invariant installation (520 Wkg^{-1}) becomes only attainable for F < 5.5%.

For A_{noz} = 1.1 m² occupation surface at the nozzle a power output between 1.65 kW and 1.85 kW is expectable from the TEG per engine within the design domain with a positive SFC impact. Under reasonable assumptions of an increased occupation surface (A_{noz} = 1.5 m²) and improved heat exchange by convection (α_H = 200 $WK^{-1}m^{-2}$, α_C = 64 $WK^{-1}m^{-2}$) the power output of the TEG increases to 2.72 kW to 3.07 kW within the design range (F < 23.8%), which shows sufficiently high gravimetric power density in order to maintain a positive SFC impact.

The resulting saving on the SFC is in the range between 0.05% and 0.1%, which translates into a considerable reduction of operation cost for the aircraft. This cost reduction opens a window for an economically efficient TEG installation. A return of invest during approximately 5 years is estimated, if the total costs of the thermoelectric recuperation system stay below 16$/W, which is a reasonable value for high performance TE materials from today's point of view.

Further improvement of the power output and the resulting SFC saving seems realistic by increase of the nozzle surface, exchange of particular materials for more performant heat transfer and by optimization of the convective heat exchange by modification of surface structures. Though, the installation of TEG in engine sections with higher temperature levels was not investigated in detail yet, it offers a significantly higher power output and SFC improvement capability compared to the nozzle installation [22]. Further studies have to verify the entire optimization potential and to clarify the possibilities for more progressive integration concepts for

TEG in aviation engines. However, the thermoelectric recuperation of waste heat of aviation jet engines provides beneficial effects to the aircraft system, due to a lowered power-offtake by the engine generator and the acceleration of the bypass flow. Consequently robust and performant TEGs could contribute to improve the fuel consumption of future aircrafts, which makes them a favorable choice, particularly with regard to other unexplored installation locations or additional positive side-effects on system level (e.g. de-icing of engine components).

Author Contributions: Conceptualization, writing—original draft preparation, project administration, and funding acquisition, P. Ziolkowski; Formal analysis, investigation, data curation, and visualization P. Ziolkowski and K. Zabrocki; Writing—review and editing, and resources P. Ziolkowski and K. Zabrocki and E. Müller; Supervision, E. Müller

Funding: This research was funded by the German Federal Ministry of Economic Affairs and Energy in the framework of Germany's fifth Aeronautical Research Program (LUFO-V), grant number 20E1303. The authors likewise thank Dr. Sieber from the MTU Aero Engines AG for the financial support.

Acknowledgments: Fruitful discussions with Ragnar Somdalen and Fabian Ahrendts from the Institute of Thermodynamics of the Technical University of Braunschweig, Christoph Bode from the Institute of Jet Propulsion and Turbomachinery of the Technical University of Braunschweig, Dragan Kožulović from the Hamburg University of Applied Science, and Kai-Daniel Büchter from Bauhaus Luftfahrt e.V. are gratefully acknowledged.

Conflicts of Interest: The authors declare no conflict of interest.

Appendix A

In order to get a more comprehensive overview on simulations and to allow readers to establish correlations between simulation results and different application boundary conditions and thermocouple designs further information is given within this supplementary information. This comprises the temperature dependent courses of transport properties (thermal conductivity, electrical conductivity and Seebeck-coefficient) considered for the p- and n-type thermoelectric materials within the simulation. The gravimetric power density in dependence of the cold side heat transfer coefficient is shown additionally, which is not discussed in the publication due to the difficulty to improve the cold side convective heat exchange without losing the positive effect on the fuel consumption by acceleration of the bypass flow. Though, technical obstacles these results confirm a significant positive impact on the gravimetric power density of the TEG, and might be helpful for prospective considerations. Additionally simulations results on the evolution of the thermocouple mass and the hot side heat flow and heat flux density, respectively, are shown as the function of the hot side heat transfer coefficient for different fill factors. Though, these results are not discussed extensively throughout the publication, they reflect central key figures of the particular TEG designs, and shall therefore be displayed within the supporting information for the sake of completeness.

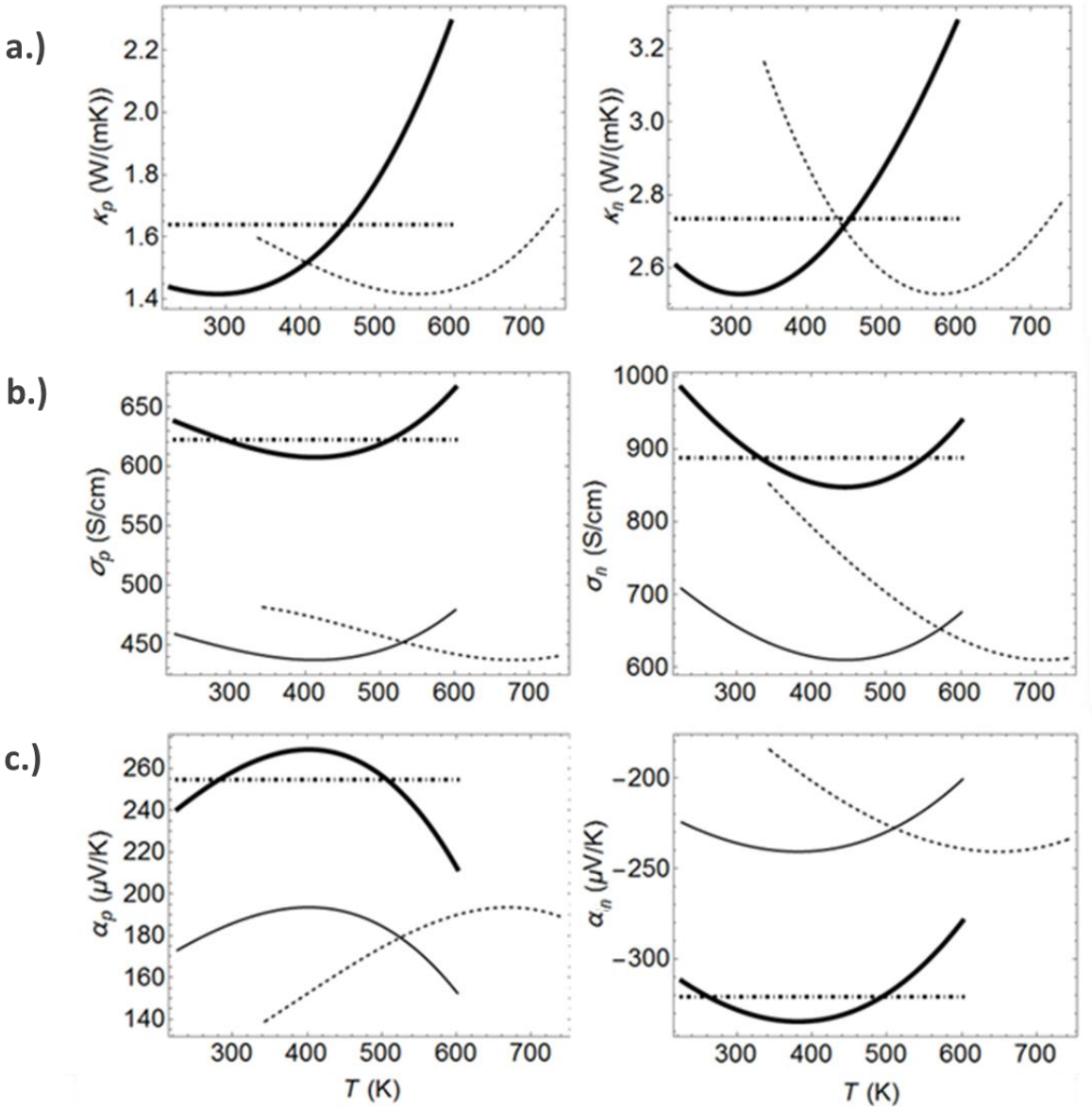

Figure A1. Material properties for the FEM simulation: Thermal conductivity (a.), electrical conductivity (b.) and Seebeck coefficient (c.) of p-type (left) and n-type (right) thermoelectric legs. The dashed lines represent fits of measured properties on Skutterudite samples. Curves shown by light solid lines show the temperature courses after the shift of transport properties into the temperature range of the nozzle application has been

applied. Bold solid lines show the property characteristics for the virtual material, which has been considered for the simulation. The broken dashed lines show the temperature mean values of the bold solid lines.

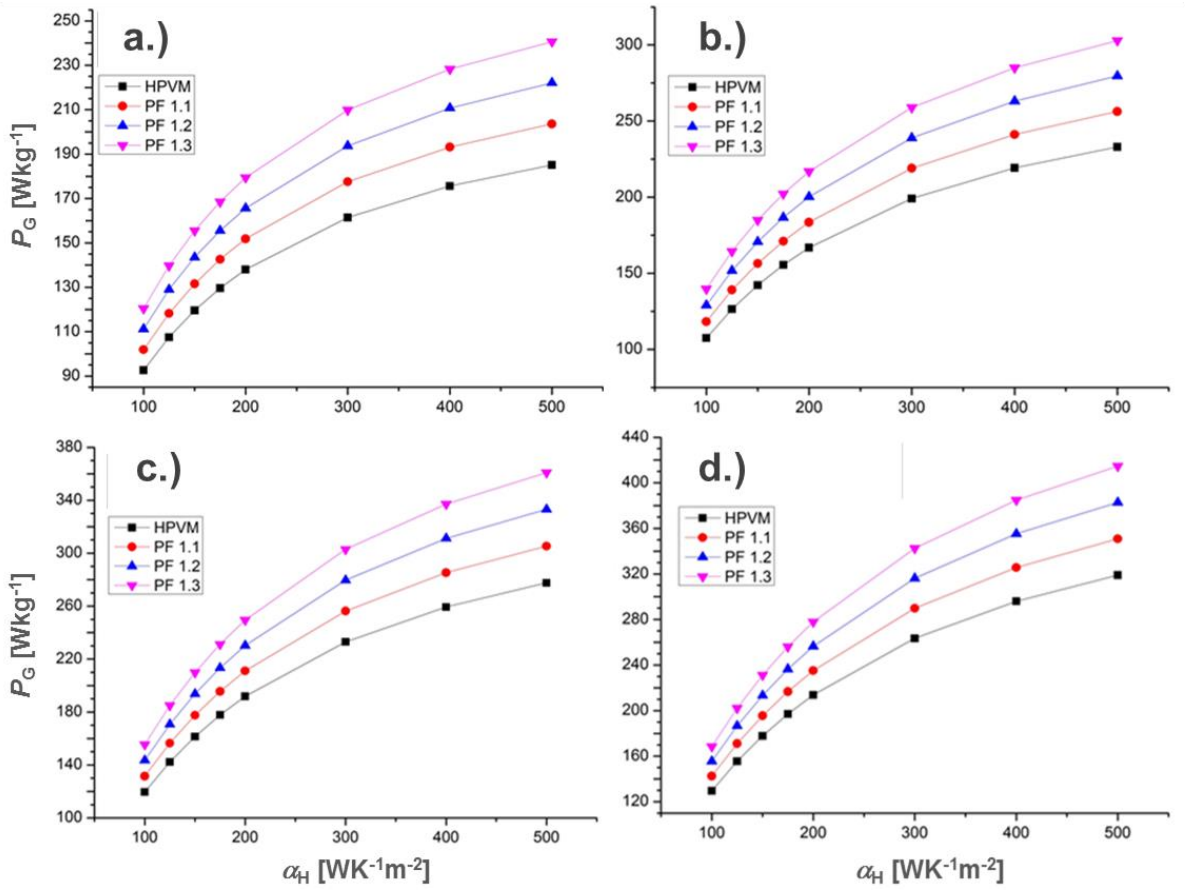

Figure A2. Gravimetric power density P_G of TEG design with a fill factor $F = 25\%$ in dependence of the convective hot side heat transfer coefficient (HTC) α_H for different cold side HTC α_C: 100 WK^{-1}m^{-2} (a.), 125 WK^{-1}m^{-2} (b.), 150 WK^{-1}m^{-2} (c.), 175 WK^{-1}m^{-2} (d.). The curves are shown for application of the high performance virtual material (HPVM) and for an increased power factor *PF* of the HPVM by three steps of 10%.

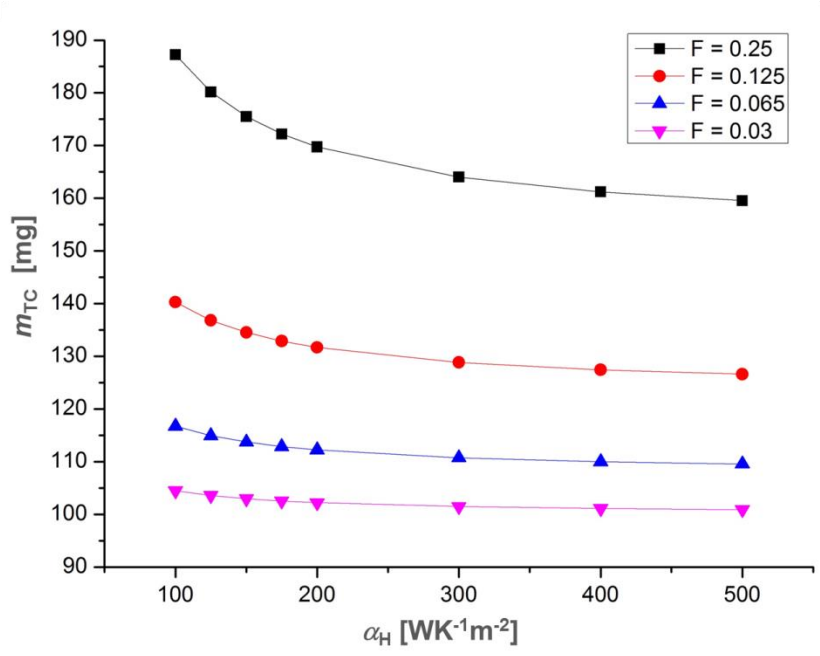

Figure A3. Thermocouple mass m_{TC} at the respective optimal leg length as a function of the hot side heat transfer coefficient α_H for different fill factors F of the thermocouple.

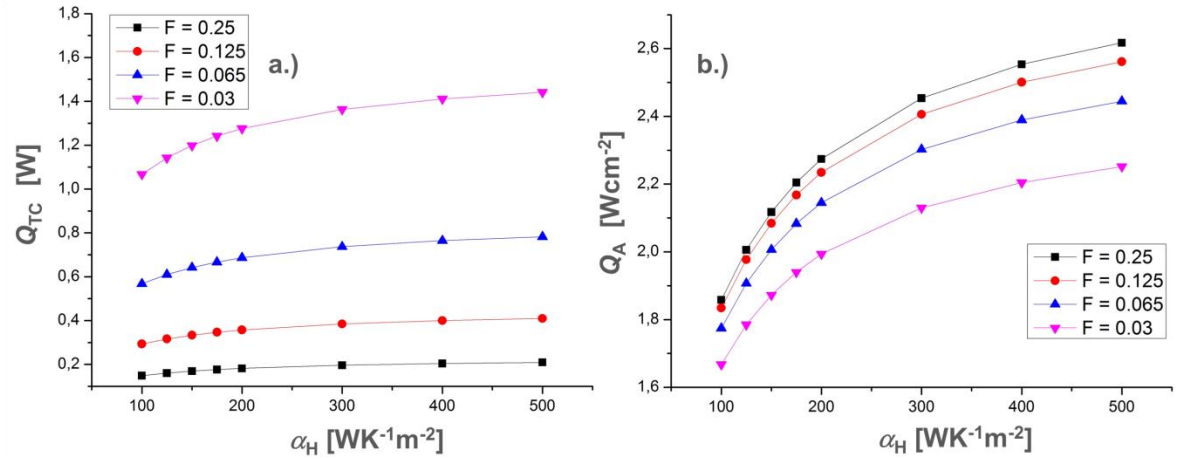

Figure A4. Incident heat flow Q_{TC} (a.) and hot side heat flux density (b.) Q_A at the respective optimal leg lengths as a function of the hot side heat transfer coefficient α_H for different fill factors F of the thermocouple.

References

1. Rowe, D.M. General Principles and Basic Considerations. In *Thermoelectric Handbook - Macro to Nano*, Rowe, D.M., Eds.; CRC Press Taylor & Francis Group: Boca Raton, USA, 2006, pp. 1.1 – 1.15, ISBN 9780849322648.
2. Yan, J.; Liao, X.; Yan, D.; Chen, Y. Review of Micro Thermoelectric Generator. *Journal of Microelectromechanical Systems* **2018**, Vol. 27, pp. 1-18, DOI: 10.1109/JMEMS.2017.2782748.
3. Yang, J.; Caillat, T. Thermoelectric Materials for Space and Automotive Power Generation. *MRS Bulletin* **2006**, Vol. 31, pp 224-229, doi:10.1557/mrs2006.49.
4. Nag S.; Dhar A.; Gupta A. Exhaust Heat Recovery Using Thermoelectric Generators: A Review. In *Advances in Internal Combustion Engine Research. Energy, Environment, and Sustainability*, Srivastava D., Agarwal A., Datta A., Maurya R., Eds.; Springer: Singapore, 2018, pp. 193-206, DOI: 10.1007/978-981-10-7575-9_10.
5. Rowe, D.M.; Smith, J.; Thomas, G.; Min, G. Weight penalty incurred in thermoelectric recovery of automobile exhaust heat. *J. Electron. Mater.* **2011**, Vol. 40, p. 784, DOI: https://doi.org/10.1007/s11664-011-1571-7.
6. Kumar, S.; Heister, S.D.; Xu, X.; Salvador, J.R.; Meisner, G.P. Thermoelectric Generators for Automotive Waste Heat Recovery Systems Part I: Numerical Modeling and Baseline Model Analysis. *J. Electron. Mater.* **2013**, Vol. 42, No. 4, p. 665, https://doi.org/10.1007/s11664-013-2471-9.
7. Ebling, D.G.; Krumm, A.; Pfeiffelmann, B.; Gottschald, J.; Bruchmann, J.; Benim, A.C.; Adam, M.; Labs, R.; Herbertz, R.R.; Stunz, A. Development of a System for Thermoelectric Heat Recovery from Stationary Industrial Processes. *J. Electron. Mater.* **2016**, Vol. 45, pp. 3433–3439, DOI: https://doi.org/10.1007/s11664-016-4511-8.
8. Kuroki, T.: Kabeya, K., Makino, K.; Kajihara, T.; Kaibe, H.; Hachiuma, H.; Matsuno, H.; Fujibayashi, A. Waste Heat Recovery in Steel Works Using Thermoelectric Generator. Proceedings of 11th European Conference on Thermoelectrics, Noordwijk, Netherlands, 2013.
9. Paradiso, J.; Starner, T. (2005). Energy scavening for mobile and wireless electronics. *IEEE Pervasive Computing* **2005**, Vol. 4, pp. 18-27, DOI: 10.1109/MPRV.2005.9.
10. Park, G.; Rosing, T.; Todd, M.D.; Farrar, C.R.; Hodgkiss, W. (2008). Energy harvesting for structural health monitoring sensor networks. *Journal of Infrastructure Systems* **2008**, Vol. 14, p. 64, DOI: https://doi.org/10.1061/(ASCE)1076-0342(2008)14:1(64).
11. Samson, D.; Otterpohl, T.; Kluge, M.; Schmid, U.; Becker, Th. Aviation-specific thermoelectric generator module. *J. Electron. Mater.* **2010**, Vol. 39, pp. 2092-2095, DOI: https://doi.org/10.1007/s11664-009-0997-7.
12. Samson, D.; Kluge, M.; Fuss, T.; Schmid, U.; Becker, Th. Flight test result of a thermoelectric energy harvester for aircraft. *J. Electron. Mater.* **2012**, Vol. 41, pp. 1134-1137, DOI: https://doi.org/10.1007/s11664-012-1928-6.
13. Dilhac, J.-M.; Bafleur, M. Energy harvesting in aeronautics for battery-free wireless sensor networks. *IEEE Aerosp. Electron. Syst. Mag.* **2014**, Vol. 29, pp. 18-22, DOI: 10.1109/MAES.2014.130002.
14. Argüelles, P.: Bischoff, M.; Busquin, P.; Droste, B.; Evans, S.R.; Kröll, W.; Lagardére, J.-L.; Lina, A.; Lumsden, J.; Ranque, D.; Rasmussen, S;, Reutlinger, P.; Robins, S.R.; Terho, H.; Wittlöv, A. *European aeronautics: A vision for 2020 - meeting societys needs and winning global leadership* **2001**. Tech. rep., European Comission.

15. Kallas, S.; Geoghegan-Quinn, M. *Flightpath2050 europe's vision for aviation - report of the high level group on aviation research* **2011**. Tech. rep., European Comission
16. Wilfert, G.; Sieber, J.; Rolt, A.; Touyeras, A.; Baker, N. New Environmental Friendly Aero Engine Core Concepts. Proceedings ISABE-2007-1120, Beijing, China, 2007.
17. Salpingidou, C., Vlahostergios, Z., Misirlis, D., Donnerhack, S., Flouros, M., Goulas, A., Yakinthos, K. Thermodynamic analysis of recuperative gas turbines and aero engines. *Applied Thermal Engineering* **2017**, Vol. 124, pp. 250-260, DOI: https://doi.org/10.1016/j.applthermaleng.2017.05.169
18. Huang, J. Aerospace and aircraft thermoelectric applications. Presentation on the DoE Thermoelectric Applications Workshop, San Diego, USA, 2009.
19. Kousksou, T. Numerical analysis of thermoelectric power generation: Aircraft systems application. Presentation on the 3rd ECOS, Lausanne, Switzerland, 2010.
20. Kousksou, T.; Bédécarrats, J.-P.; Champier, D.; Pignolet, P.; Brillet, C. Numerical study of thermoelectric power generation for an helicopter conical nozzle. *Journal of Power Sources* **2011**, Vol. 196, pp. 4026-4032, DOI: https://doi.org/10.1016/j.jpowsour.2010.12.015
21. Pace GmbH: Pacelab APD3.0 User Documentation, 2011.
22. Bode, C.; Friedrichs, J.; Somdalen, R.; Köhler, J.; Büchter, K.-D.; Falter, C.; Kling, U.; Ziolkowski, P.; Zabrocki, K.; Müller, E.; Kožulović, D. Potential of Future Thermoelectric Energy Recuperation for Aviation. *J. Eng. Gas Turbines Power* **2017**, Vol. 139(10), p. 101201, DOI: 10.1115/1.4036527.
23. Bode, C.; Friedrichs, J.; Ahrendts, F.; Lemke, N.; Köhler, J.; Kozulovic, D. Numerical Flow Simulation of Heat Recuperation in the Exhaust Section of a Turbofan Engine. Proceedings of 53rd AIAA/SAE/ASEE Joint Propulsion Conference, AIAA Propulsion and Energy Forum, (AIAA 2017-5033), Atlanta, USA, 2017, DOI: https://doi.org/10.2514/6.2017-5033.
24. Kurzke, J. GasTurb 12, Design and Off-Design Performance of Gas Turbine Engines, 2013 www.gasturb.de/Gtb12Manual/GasTurb12.pdf, (accessed on 01.11.2018).
25. Kügeler, E. Numerisches Verfahren zur genauen Analyse der Kühleffektivität filmgekühlter Turbinenschaufeln. PhD Thesis, Ruhr-University Bochum, Bochum, Germany, 2005-11.
26. Marciniak, V.; Kügeler, E.; Franke, M. Predicting Transition on Low-Pressure Turbine Profiles. Proceedings of V. European Conference on Computational Fluid Dynamics, Lisbon, Portugal, 2010.
27. Becker, K.; Heitkamp, K.; Kügeler, E.. Recent Progress in a Hybrid-Grid CFD Solver for Turbomachinery Flows. Proceedings of V. European Conference on Computational Fluid Dynamics, Lisbon, Portugal, 2010.
28. Büchter, K.-D.; Kling, U.; Bode, C.; Friedrichs, J. Estimation of mission fuel saving potential using thermoelectric recuperation in aero-engines. *Transportation Research Procedia* **2018**, Vol. 29, pp. 23–33, DOI: https://doi.org/10.1016/j.trpro.2018.02.003.
29. Bartolotta, P.; Barrett, J.; Kelly, T.; Smashey, R. The Use of Cast Ti-48Al-2Cr-2Nb in Jet Engines. *Journal of Material* **1997**. Vol. 76, pp. 48-50, DOI: https://doi.org/10.1007/BF02914685.
30. Junior, A.F.; Shanafield, D.J. Thermal conductivity of polycrystalline aluminum nitride (AlN) ceramics. *Ceramica* **2004**, Vol. 50, pp. 247-253, DOI: http://dx.doi.org/10.1590/S0366-69132004000300012.
31. CoorsTek GmbH: AlN Technical Datasheet, 2016, https://www.coorstek.com/media/1909/aluminum-nitride-aln-brochure.pdf, (accessed on 01.11.2018).
32. Thapliyal, P.C.; Singh, K. Aerogels as Promising Thermal Insulating Materials: An Overview. *Journal of Materials* **2014**, Vol. 2014, pp. 1-10 , DOI:10.1155/2014/127049.
33. Aspen Aerogels: Datasheet of Pyrogel XT, 2008, http://arrowheadcontractorsupply.com/Pyrogel_XT_DS.pdf, (accessed on 01.11.2018).
34. Baranowski, L.L.; Snyder, J.G.; Toberer, E.S. Effective thermal conductivity in thermoelectric materials, *Journal of Applied Physics* **2013**, Vol. 113, 204904, DOI: https://doi.org/10.1063/1.4807314.
35. Lundbladh, A.; Grönstedt, T.; Genrup, M.; Platell, P. High power density work extraction from turbofan exhaust heat. Proceedings of 22nd International Symposium on Air Breathing Engines, Phoenix, USA, 2015.
36. Bennett, G.L.; Lombardo, J.J.; Hemler, R.J.; Silverman, G.; Whitmore, C.W.; Amos, W.R.; Johnson, E.W.; Schock, A.; Zocher, R.W.; Keenan, T.K.; Hagan, J.C.; Englehart, R.W. Mission of Daring: The General-Purpose Heat Source Radioisotope Thermoelectric Generator. Proceedings of the 4th International Energy Conversion Engineering Conference and Exhibit (IECEC), Paper AIAA 2006–4096, American Institute of Aeronautics and Astronautics, San Diego, USA, 2006.
37. Yazawa, K.; Shakouri, A. Cost-Efficiency Trade-off and the Design of Thermoelectric Power Generators. *Environ. Sci. Technol.* **2011**, Vol. 45, pp. 7548–7553, DOI: 10.1021/es2005418.

38. Semenyuk, V. A Comparison of Performance Characteristics of Multistage Thermoelectric Coolers Based on Different Ceramic Substrates. *J. Electron. Mater.* **2014**, Vol. 43, pp. 1539–1547, DOI: https://doi.org/10.1007/s11664-013-2777-7.
39. Böttner, H.; Nurnus, J. Miniaturized Thermoelectric Converters, Technologies and Applications. In *Thermoelectrics and its Energy Harvesting, Vol. 2, Modules, Systems, and Applications in Thermoelectrics*, Rowe, D.M. (Ed.); CRC Press Taylor & Francis Group: Boca Raton, USA, 2012, pp. 17.1 – 17.18, ISBN 9781439840412.
40. Büchter, K.D. (Bauhaus Luftfahrt e.V., Munich, Bavaria, Germany). Personal communication, 2017.
41. Dames, C. Cost optimization of thermoelectric materials for power generation: The case for ZT at (almost) any cost. *Scripta Materialia* **2016,** Vol. 111, pp. 16–22, DOI: https://doi.org/10.1016/j.scriptamat.2015.06.018.
42. LeBlanc, S.; Yee, S.K.; Scullin, M.L.; Dames, C.; Goodson, K.E. Material and manufacturing cost considerations for thermoelectrics. *Renewable and Sustainable Energy Reviews* **2014**, Vol. 32, pp. 313–327, DOI: https://doi.org/10.1016/j.rser.2013.12.030.